Available online at www.sciencedirect.com
ScienceDirect
Trans. Nonferrous Met. Soc. China 32(2022) 3998−4013
Transactions of Nonferrous Metals Society of China
www.tnmsc.cn

Corrosion evolution of high-temperature formed oxide film on pure Sn solder substrate

Hui ZHAO[1], Xu SUN[1,2], Long HAO[2,3], Jian-qiu WANG[2,3], Jing-mei YANG[4]

1. School of Materials Science and Engineering, Shenyang Ligong University, Shenyang 110159, China;
2. CAS Key Laboratory of Nuclear Materials and Safety Assessment, Institute of Metal Research, Chinese Academy of Sciences, Shenyang 110016, China;
3. School of Materials Science and Engineering, University of Science and Technology of China, Hefei 230026, China;
4. Shenyang Aircraft Industry (Group) Corporation Ltd., Shenyang 110034, China

Received 30 September 2021; accepted 19 November 2021

Abstract: The evolution of morphology, composition, thickness and corrosion resistance of the oxide film on pure Sn solder substrate submitted to high-temperature aging in 150 °C dry atmosphere was investigated. The results indicate that high-temperature aging accelerates the dehydration of $Sn(OH)_4$ in the pre-existing native oxide film to form SnO_2 and facilitates the oxidation of fresh Sn substrate, resulting in the gradual increase in oxide film thickness and surface roughness with prolonging aging time. However, the corrosion resistance of the film initially is enhanced and then deteriorated with an extending aging time. Besides, the formation and evolution mechanisms of the oxide film with aging time were discussed.

Key words: pure Sn solder; oxide film; high-temperature aging; corrosion resistance

1 Introduction

As connection materials, Sn-based solder alloys have always been at the dominant position in electronic packaging industry [1,2]. However, the widely used Sn−Pb solders over the past several decades have been restricted due to the toxicity of Pb element to human health and environment, and thus the Sn-based Pb-free solder alloys have been in development worldwide [3,4]. Nowadays, the Sn-based Pb-free solders have occupied a substantial market share in electronic packaging industry [5], and kinds of binary or ternary solder alloys for different application purposes have been developed, such as Sn−Ag [6], Sn−Cu [7] and Sn−Ag−Cu [8]. During the practical applications of Sn solder alloys, Sn substrate is prone to oxidize and thus the presence of a surface oxide film is unavoidable. Interestingly, the physicochemical characteristics of the oxide film can shape the engineering performance of Sn solder joints [9]. As to the surface oxide film formation mechanism, manners of chemical oxidation and electrochemical oxidation have been proposed [10−12]. In humid atmosphere with a higher relative humidity (RH), the water vapor can interact with Sn substrate, producing Sn^{2+} that further undergoes processes of hydrolysis, dehydration and oxidation to form an electrochemically inactive SnO_2 film as a function of exposure time [9]. In dry atmosphere with a relatively high temperature, the depletion of water vapor and high temperature environment make Sn substrate to be oxidized directly by oxygen to form SnO_2 film [11]. Although both the electrochemical oxidation in humid atmosphere and the direct chemical oxidation in high-temperature environment will finally contribute to oxide films with the same

Corresponding author: Long HAO, Tel: +86-24-23998826, E-mail: chinahaolong@126.com, lhao@imr.ac.cn
DOI: 10.1016/S1003-6326(22)66073-4

composition of SnO_2, the film morphology, compactness, thickness and corrosion resistance may vary significantly, leading to variation in protectiveness of the oxide film to underlying solder substrate [13,14].

It is usually believed that SnO_2 is a composition of high thermodynamic stability with better resistance in the presence of corrosion electrolyte, and a compact SnO_2 layer can well protect Sn solder substrate from corrosion electrolyte attack [15]. Nevertheless, it should be noticed that the advances in packaging technology have led to the miniaturization trends to manufacture continually smaller electronic devices with increased power density [16]. Consequently, the long-term excessive heat release by electronic device itself during working will definitely deteriorate the structure and corrosion resistance of the oxide film, and also cause oxidation in the fresh substrate, further complicating the evolutions in composition, thickness and structures of the oxide film. Moreover, microcracks are also prone to form in a thicker oxide film due to the increasing inner stress [17]. Therefore, even with a thicker oxide film, the pores or cracks in oxide film may lower its resistance to corrosion attack.

To the best of our knowledge, research on Sn solder alloys is mainly focused on micro-structure optimization and mechanical property improvement [18−21]. Nevertheless, the high-temperature aging time induced evolutions in morphology, composition and corrosion resistance of the surface oxide film have rarely gained much attention. In this work, the surface oxide film on pure Sn solder substrates was firstly prepared by exposing the substrates to 150 °C high-temperature environment with aging time as a parameter, and then scanning electron microscopy (SEM), laser scanning confocal microscopy (LSCM) and X-ray photoelectron spectroscopy (XPS) were employed to characterize the evolutions of morphology, roughness and composition of the film. Finally, the corrosion resistance evolution of the oxides film was discussed by potentiodynamic polarization curves and electrochemical impedance spectroscopy (EIS). The expected findings are vital in exploring the structure and corrosion behavior of the high-temperature formed oxide film on Pb-free Sn solder joint surface.

2 Experimental

2.1 Sample preparation and high-temperature aging process

The pure Sn solder bars (in purity of 99.9%) were purchased from Shenzhen Huacheng Solder Technology Co., Ltd., China. Sn bars were kept at 300 °C for 0.5 h with the aid of stainless steel mould and then cooled in furnace to ambient temperature to simulate the solder joints after welding. Then, the obtained sample was cut into blocks of 10 mm × 10 mm × 5 mm in size and the sample surface was ground by sandpapers from 400 to 5000 grit sequentially. Finally, the sample surface was polished by 1 μm diamond polishing paste and by 0.05 μm SiO_2 suspension, rinsed by deionized water, and then dried in a steam of room temperature air for tests.

The heating cabinets (PH−250), provided by Shanghai Suying Test Instrument Co., Ltd., China, were run, and the temperature was set at 150 °C. The prepared pure Sn substrates were exposed to the high-temperature environment for durations of 2, 4, 6 and 8 d to obtain oxide films with different structures. Meanwhile, Sn substrate without high-temperature aging was also investigated for comparison.

2.2 Surface morphology and roughness analyses

The evolution in surface morphology of high-temperature aged Sn solder substrate with aging time as a parameter was characterized by means of a scanning electron microscope (SEM, Philips XL30 FEG), equipped with EDS for element analysis. In addition, the evolution in surface roughness at the same position as a function of aging time was characterized by means of a laser scanning confocal microscope (LSCM, LSM700), with scanning step of 0.1 μm. The obtained parameter of average surface roughness (S_a) can reflect the oxide film surface roughness evolution with the high-temperature aging time.

2.3 Composition and structure analyses

The composition evolution of oxide film on the solder surface was characterized by an X-ray photoelectron spectroscope (XPS, ESCALAB250) using a monochromatic Al K_α X-ray excitation source ($h\nu$=1486.6 eV), and the spot area was

100 μm in diameter. Survey spectra were recorded and high-resolution spectra of Sn 3d and O 1s core level regions were collected at 0° with respect to normal at different sputtering depths to reveal the in-depth profile of composition in the oxide film. The deconvolution of high-resolution spectra was performed with the XPS peak 4.1 software using an iterative Shirley-type background subtraction under Gaussian/Lorentzian functions after peak calibration to standard C 1s signal at 284.6 eV.

2.4 Electrochemical measurements

The electrochemical impedance spectroscopy (EIS) and potentiodynamic polarization curve measurements have also been employed to evaluate the corrosion evolution behavior of the high-temperature aged Sn solder substrates covered with an oxide film in 3.5 wt.% NaCl solution, and Gamry Reference 600 electrochemical workstation was employed. Three-electrode system was used with the high-temperature aged Sn solder substrates (covered with oxide film) as working electrode, platinum foil with 4 cm^2 area as counter electrode, and saturated calomel electrode (SCE) as reference electrode. The working electrode was immersed in electrolyte for 2 h to obtain a stabilized open circuit potential (OCP), and then EIS data were recorded in the frequency range from 100 kHz to 10 mHz with ±5 mV exciting signal. After that, the polarization curve was recorded in the potential range from −0.15 to 0.5 V (vs OCP) with a scan rate of 0.167 mV/s at room temperature to evaluate the corrosion resistance of the oxide film. The fitting of EIS data was performed using Zsimpwin software.

3 Results and discussion

3.1 Surface morphology evolution

The evolution in surface morphology of pure Sn solder substrate exposed to 150 °C dry atmosphere with aging time is shown in Fig. 1. Obviously, for the sample without high-temperature aging in Fig. 1(a), the surface is clean and smooth. However, as the aging time proceeds, a gravel-like

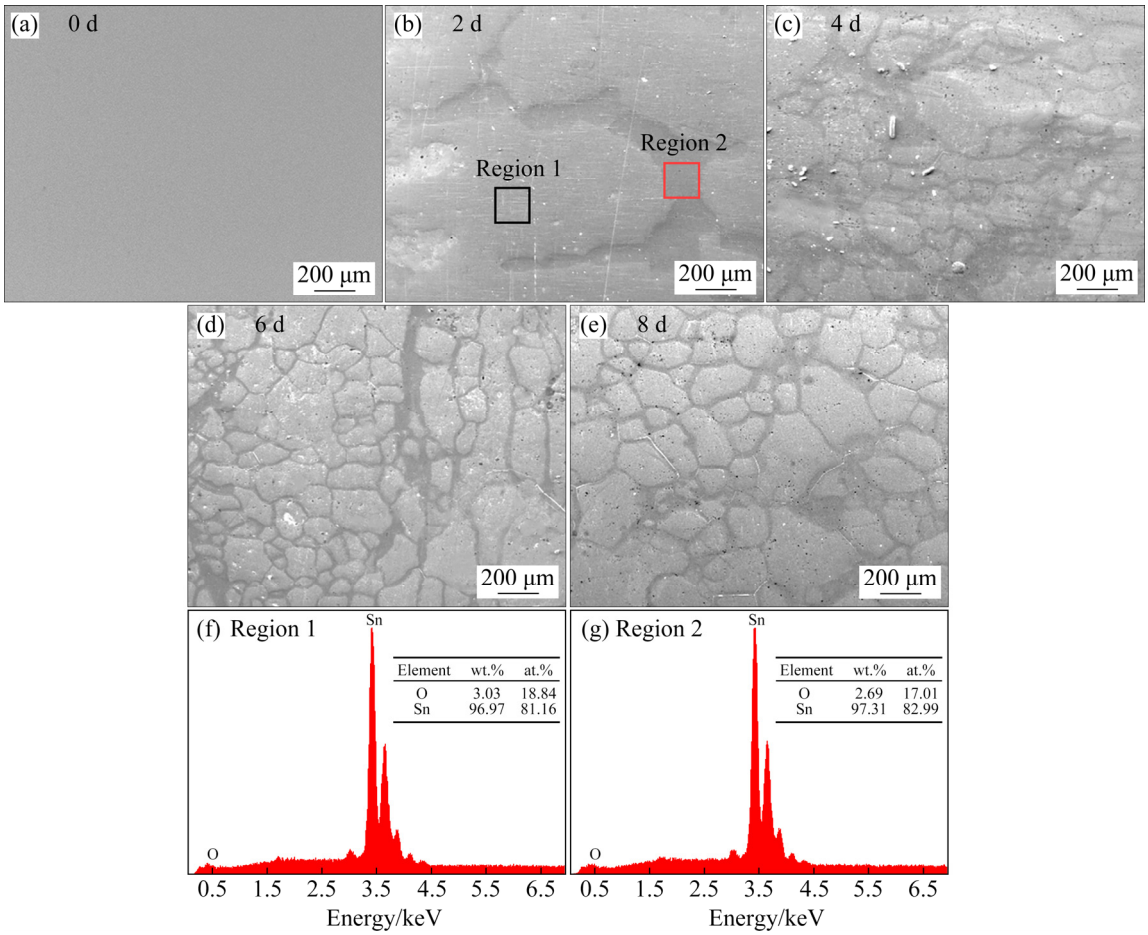

Fig. 1 Evolution of surface morphology of oxide film obtained on pure Sn solder substrate exposed to 150 °C dry atmosphere with aging time (a−e) and EDS spectra of local areas (f, g)

rough surface morphology has been observed with the gravel diameter being varied as seen from Fig. 1(b) to Fig. 1(e). Therefore, the surface morphology of the pure Sn solder surface evolves predominantly as the aging time proceeds, indicating the pronounced effect of high-temperature aging time on the surface morphology of pure Sn solder substrate.

It is widely accepted that a native (natural formed) oxide film forms in a very short duration on Sn solder substrate surface even in room-temperature indoor atmosphere [12], and thus it is expected that there is an oxide film existing on the sample without high-temperature aging in Fig. 1(a), even if a smooth and uniform surface has been observed. Usually, this native oxide film has a layered structure with stannic compounds enriched in the outer layer and stannous compounds in the inner layer [22], and the content ratio of hydroxides to oxides in the film varies depending on temperature and relative humidity RH of the exposure environment [10,23]. After being exposed to 150 °C dry atmosphere, the hydroxides can be dehydrated to form oxide films with water molecules being released [24]. Therefore, a gravel-like rough surface has been observed for the oxide film sample with an aging time of 2 d in Fig. 1(b). EDS has been employed to detect the elements difference between Region 1 and Region 2 as indicated by square markers in Fig. 1(b). It is found from Fig. 1(f) and Fig. 1(g) that both Sn element and O element have the same level in content in the two regions, indicating that the region on top of gravels and the region at interface of gravels have almost the same composition without difference. When the aging time proceeds to 4 d, the morphology in Fig. 1(c) also shows a gravel-like rough surface of the oxide film but with a much smaller diameter of the gravels. It is supposed that further dehydration of native oxide film and the oxidation of fresh Sn solder substrate may be responsible for such a deterioration [25]. Moreover, for the samples with an aging time of 6 and 8 d, the corresponding morphologies in Fig. 1(d) and Fig. 1(e) possess similar characteristics with the 4 d sample in Fig. 1(c), indicating the accomplishment of native oxide film dehydration during the initial 4 d aging and further oxidation of fresh Sn solder substrate with an extending aging time [26].

LSCM has been employed to characterize the evolution in surface roughness of the oxide film on pure Sn solder substrate with high-temperature aging time, and the results are shown in Fig. 2. It is necessary to claim that the results in Fig. 2 are observed in the same area of interest as a function of aging time. Obviously, for the as-obtained native Sn solder substrate sample without high-temperature aging in Fig. 2(a), it has a lower value of surface roughness of S_a=74 nm, indicating the uniform formation of native oxide film on Sn solder substrate surface. However, an aging time of 2 d leads to a rough surface of the oxide film with S_a=112 nm in Fig. 2(b), and this sharply increased roughness value indicates that the native oxide film

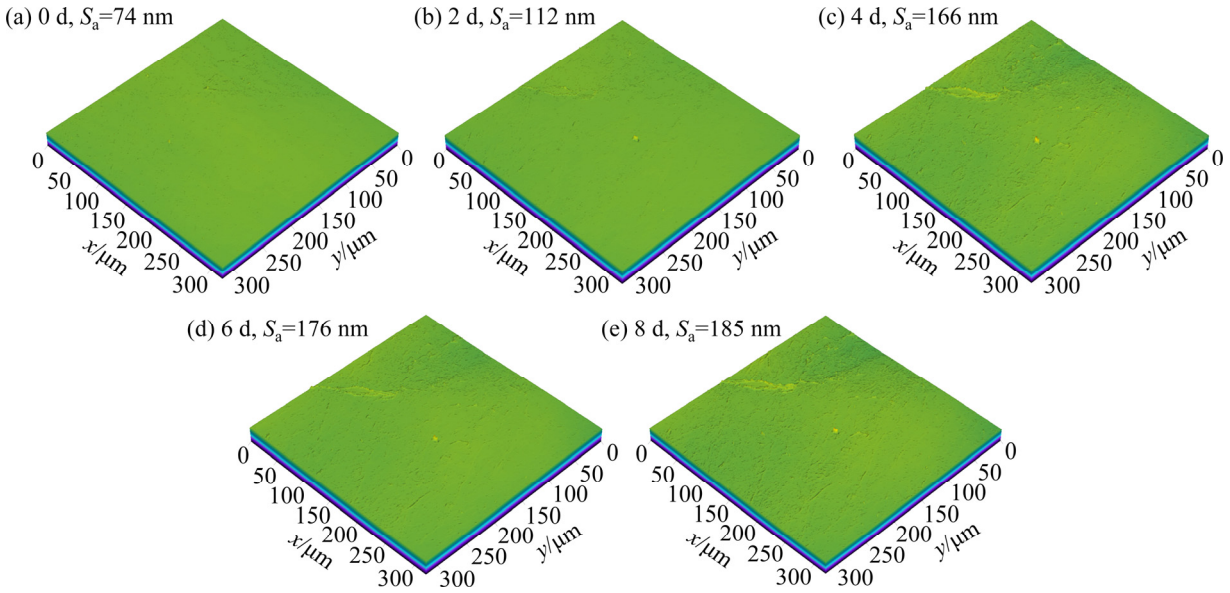

Fig. 2 Evolution of surface roughness (S_a) of oxide film obtained on pure Sn solder substrate surface with high-temperature aging time in 150 °C dry atmosphere

deteriorates greatly during the initial 2 d aging. When the high-temperature aging proceeds to 4 d, the surface roughness of the oxide film again increases to a much higher value of S_a=166 nm in Fig. 2(c), and the further dehydration of native oxide film and the oxidation of fresh Sn solder substrate may be responsible for this [27]. However, for the sample with an aging time of 6 d, it has a surface roughness value of S_a=176 nm; for the sample with an aging time of 8 d, it has a surface roughness value of S_a=185 nm, indicating that the dehydration of native oxide film has finished during the initial 4 d aging and the oxidation of fresh solder substrate further proceeds with an extending aging time. Therefore, the surface roughness evolution results in Fig. 2 are in accordance with the surface morphology observation in Fig. 1.

3.2 Composition evolution by XPS analyses

XPS has been employed to understand the structure of the surface oxide film on pure Sn solder substrate, and constituent elements of Sn and O are detected in all the spectra. Figure 3 gives the high-resolution spectra of Sn $3d_{5/2}$ and O 1s and their corresponding deconvolution results obtained on the top surface of the oxide film without depth sputtering. The binding energies (E_b) at line position for Sn $3d_{5/2}$ and O 1s spectra deconvolution are used to identify the chemical state of Sn and O elements in the oxide film, and the extracted data of full width at the half-line maximum (FWHM) for each sub-spectrum are both listed in Table 1.

The symmetry of the high-resolution spectra for Sn $3d_{5/2}$ peaks in Fig. 3(a) and the deconvolutions show that only one sub-peak in binding energy range of 486.1−486.4 eV has been observed and it is recognized as the state of Sn^{4+} in stannic oxide lattice [28]. However, the asymmetry of the high-resolution spectra for O 1s peaks in Fig. 3(b) and the deconvolutions demonstrate that the contained O element has two states, i.e., the metallic oxides and hydroxides [29]. Analyses indicate that the sub-peak in range of 530.2−530.6 eV is supposed to be the state of O^{2-} in the Sn-oxide lattice ($(O^{2-})_{lattice}$), and the sub-peak in range of 531.6−531.8 eV is regarded as the state of OH^- in Sn-hydroxide lattice ($(OH^-)_{lattice}$) [30]. Therefore, it can be concluded that for the oxide film on pure Sn solder substrate submitted to high-temperature aging at 150 °C for 2, 4, 6 and 8 d, its most surficial layer is composed of SnO_2 and $Sn(OH)_4$. As to the content ratio of SnO_2 to $Sn(OH)_4$, it can be reflected by peak area ratio of $(O^{2-})_{lattice}/(OH^-)_{lattice}$ that could be deduced from the fitted sub-peak area, and Fig. 4 indicates that the $(O^{2-})_{lattice}/(OH^-)_{lattice}$ ratio has a value of 1.51 for the 2 d aged sample and it increases to about 1.71 for the sample with an aging time of 8 d. Such a ratio much higher than 0.5 demonstrates that $Sn(OH)_4$ always takes a much lower content than SnO_2 in the most surficial layer of the oxide film on pure Sn solder substrate.

The above XPS data obtained without depth sputtering on the oxide film surface only provide compositional information in the oxide film with a depth less than 5 nm [31]. To understand composition of the inner oxide film layer, a series of XPS data as a function of sputtering depth from the oxide film surface have been recorded, and Fig. 5 gives the XPS data obtained at a depth about 6 nm (sputter rate 0.1 nm/s, time 60 s) in the oxide film. Obviously, the asymmetry of the high-resolution spectra for Sn $3d_{5/2}$ peaks in Fig. 5(a) demonstrates that Sn element no longer has only one chemical state. Besides the Sn^{4+} sub-peak in the range of 486.1−486.4 eV, deconvolutions show that the sub-peak in range of 484.9−485.2 eV is attributed to Sn^{2+} in the stannous oxide lattice [32], and the sub-peak at about 484.4 eV is caused by metallic Sn from Sn solder substrate [33]. However, the deconvolution of high-resolution spectra for O 1s peaks in Fig. 5(b) only indicates the presence of O^{2-} caused by Sn-oxides lattice ($(O^{2-})_{lattice}$) in inner layer of the oxide film. Therefore, it can be concluded that for the oxide film on pure Sn solder substrate submitted to high-temperature aging at 150 °C for 2, 4, 6 and 8 d, the inner layer of the oxide film is composed of SnO_2 and SnO. To understand the relative content of SnO_2 and SnO in inner layer of the oxide film with different aging time, Fig. 6 shows the relative peak areas of Sn^{4+} and Sn^{2+} sub-peaks calculated from the deconvolution of high-resolution spectra in Fig. 5(a). Obviously, at the oxide film depth with a sputtering time of 60 s, the relative content of SnO_2 gradually increases and that of SnO decreases gradually as the aging time proceeds from 2 to 8 d, indicating the increasing thickness of the oxide film as a function of aging time, and SnO_2 mainly locating in outer layer of the oxide film and SnO locating in the inner layer.

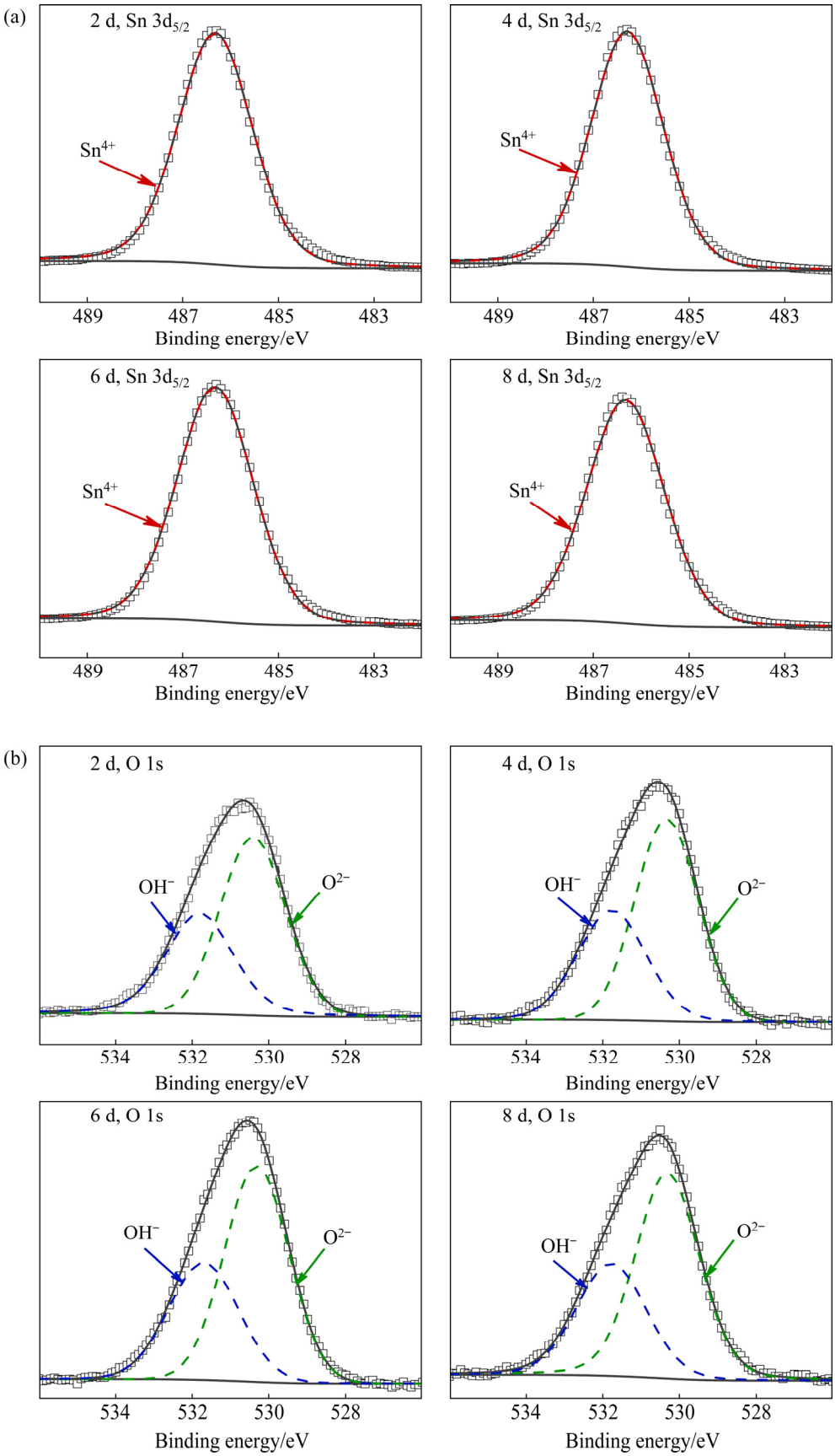

Fig. 3 High-resolution spectra of Sn $3d_{5/2}$ (a) and O 1s (b) and their corresponding deconvolution results obtained on top surface of oxide film without sputtering depth on pure Sn solder substrate surface with high-temperature aging time in 150 °C dry atmosphere

Table 1 Binding energy (E_b) at line position used for analyzing XPS spectra of surface oxide film on high-temperature aged pure Sn solder substrates, together with full width at half-line maximum (FWHM) extracted by deconvolution

Species	Chemical state	E_b/eV	FWHM/eV
Sn^{4+}	Sn $3d_{5/2}$	486.1−486.4	1.33−1.91
Sn^{2+}	Sn $3d_{5/2}$	484.9−485.2	1.07−1.43
Sn^{0}	Sn $3d_{5/2}$	484.4−484.8	1.10−1.23
O^{2-}	O 1s	530.2−530.6	1.50−2.54
OH^{-}	O 1s	531.6−531.8	1.95−2.22

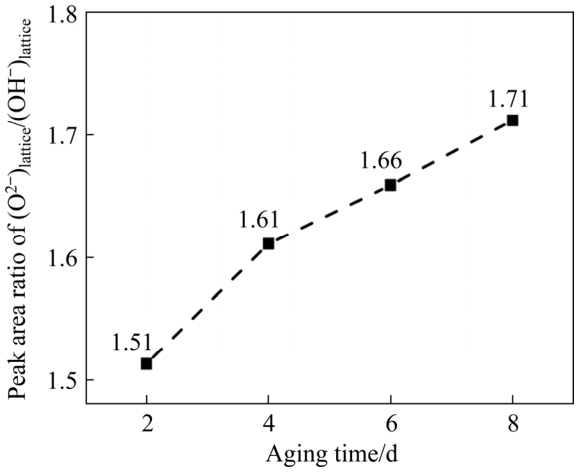

Fig. 4 Evolution of peak area ratio of $(O^{2-})_{lattice}/(OH^{-})_{lattice}$ collected from O 1s XPS spectra obtained on top surface of oxide film without depth sputtering on pure Sn solder substrate with high-temperature aging time in 150 °C dry atmosphere

The thickness evolution of the oxide film on pure Sn solder substrate surface as a function of high-temperature aging time has been determined by molar fraction of O element from the XPS spectra as sputtering depth proceeds, and it is shown in Fig. 7. Analyses show that the derived thickness of oxide film on pure Sn solder substrate with an aging time of 2, 4, 6 and 8 d is 6, 7, 9 and 13 nm, respectively. To clearly demonstrate the evolution trend in thickness value of the oxide film, Fig. 8 shows the derived thickness value as a function of high-temperature aging time. Obviously, the oxide film thickens less during the initial 4 d, and then grows quickly as the aging time further proceeds, especially during the interval from 6 to 8 d. It is believed that such an evolution behavior in growth kinetics of the oxide film thickness is related to the deterioration of pre-existing native oxide film and the oxidation of fresh Sn substrate as the aging time proceeds.

3.3 Electrochemical measurements

3.3.1 Evolution of electrochemical impedance spectrum

The above characterization indicates that high-temperature aging time has a substantial effect on morphology, composition and thickness of the oxide film on pure Sn solder substrate as a function of aging time. To investigate the evolution in corrosion resistance of the oxide film with the aging time, EIS characterization of the high-temperature aged samples with different aging time was performed in 3.5 wt.% NaCl solution, and the results are shown in Fig. 9. It can be seen from Fig. 9(a) that the impedance at high frequency ($|Z|_{HF}$) caused by solution resistance (R_s) varies little as the aging time proceeds. Within the frequency (f) range of 10^3−10^1 Hz, a lower slope value of curve of $\lg|Z|$ versus $\lg f$ for the sample without high-temperature aging compared with the aged ones has been observed, indicating the poor corrosion resistance of the pre-existing native oxide film. Meanwhile, the observed slope value higher than −1.0 indicates the presence of a constant phase element (CPE), and under this situation the measured electrochemical impedance response is mainly caused by the surface oxide film [34,35]. Besides, the low frequency impedance ($|Z|_{LF}$) firstly increases and then decreases as the aging time proceeds, indicating the substantial effect of high-temperature aging on corrosion resistance of the pure Sn solder substrate. For the phase angle evolution in Fig. 9(b), its profile varies greatly as the aging time proceeds, indicating the significant influence of high-temperature aging time on structures of the oxide film, as the phase angle evolution is always sensitive to oxide film structure [36]. For the pre-existing native oxide film without high-temperature aging, it shows a lower constant value during a relatively narrow frequency range. However, for the samples with aging time of 2 and 4 d, a larger phase angle value close to −85° in a broader frequency range of 10^3−10^0 Hz has been observed, indicating the enhanced corrosion resistance of the two samples compared with the one without high-temperature aging. In this case, the EIS data will be fitted by an equivalent electrical

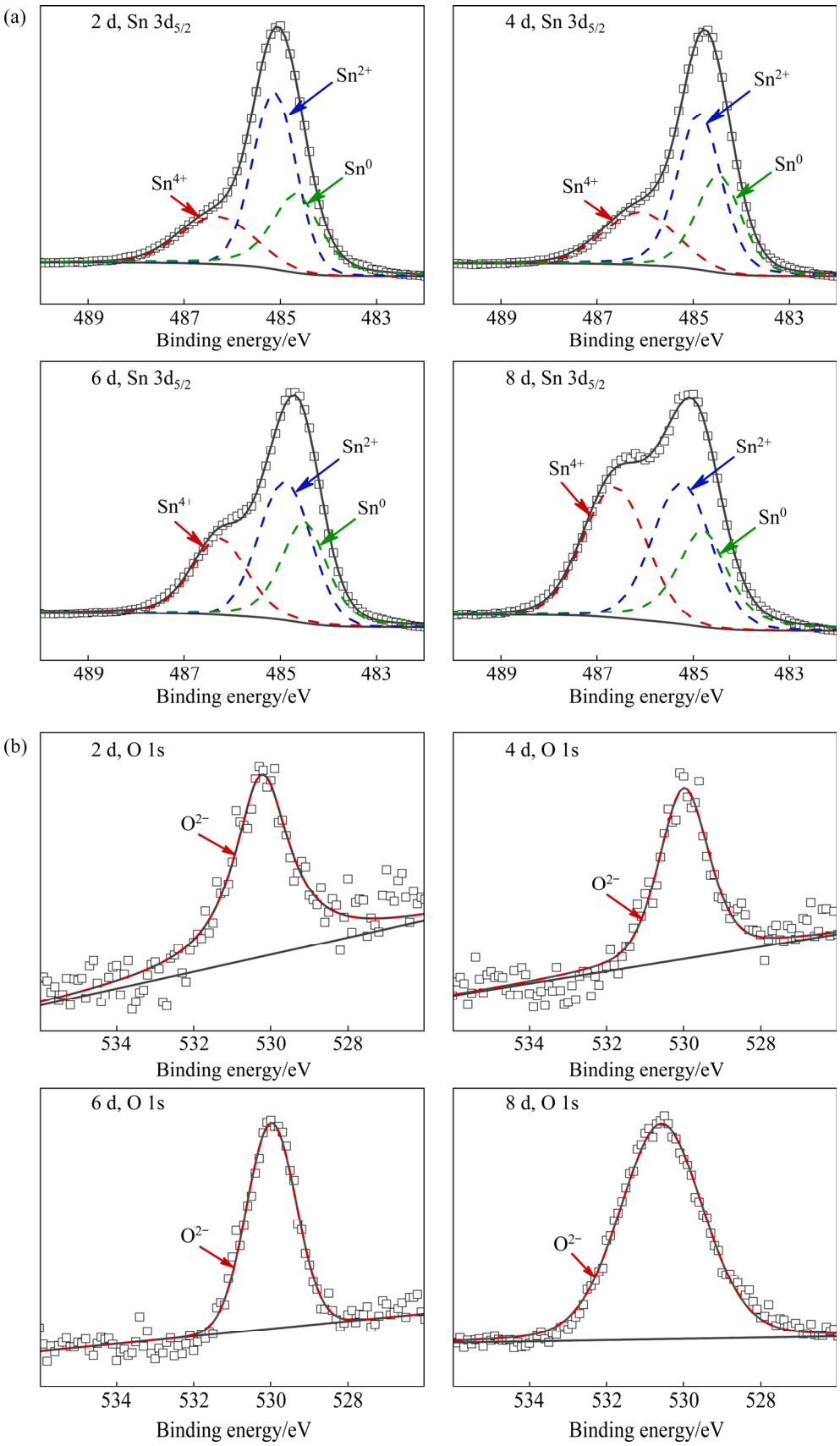

Fig. 5 High-resolution spectra of Sn $3d_{5/2}$ (a) and O 1s (b) and their corresponding deconvolution results obtained at sputtering depth of about 6 nm in oxide film on pure Sn solder substrate surface with high-temperature aging time in 150 °C dry atmosphere

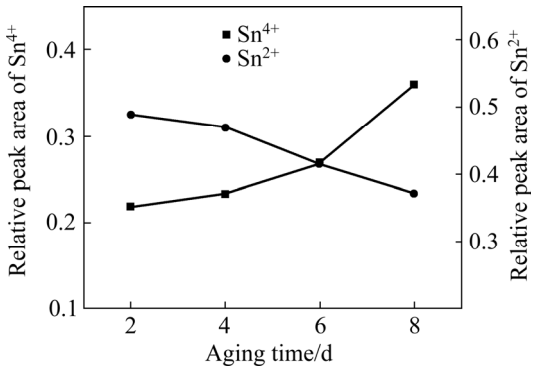

Fig. 6 Relative peak areas of Sn^{4+} and Sn^{2+} calculated from deconvolution of high-resolution spectra obtained at sputtering depth of about 6 nm in oxide film on pure Sn solder substrate with high-temperature aging time in 150 °C dry atmosphere

circuit (EEC) with one time-constant being considered in Fig. 10(a). For the samples with extending aging time of 6 and 8 d, the phase angle profile in the higher-frequency range changes little, but the profile in the lower-frequency range evolves greatly, indicating a great deterioration in the oxide film structure of the samples with extending aging time of 6 and 8 d. Therefore, an EEC in Fig. 10(b) with two time-constants will be used for the EIS data fitting.

In Fig. 10(a), R_s is the electrolyte resistance, and constant phase element CPE_{os} and R_{os} reflect pseudo capacitance and Faraday resistance of the oxide film, respectively. Therefore, the combination of R_{os} in parallel with CPE_{os} represents the dielectric property of oxide film. In Fig. 10(b), constant phase element CPE_{outer} and R_{outer} reflect pseudo capacitance and resistance of the outer layer of the oxide film, respectively. The constant phase element CPE_{inner} and R_{inner} reflect the capacitance and resistance of the inner layer of the oxide film, respectively. In this situation, in Fig. 10(b), $R_{outer}+R_{inner}=R_{os}$. Moreover, the impedance function Z_ω for Fig. 10(a) and Fig. 10(b) can be expressed by Eq. (1) and Eq. (2), respectively:

$$Z_\omega = R_s + \frac{1}{j\omega Q_{os} + 1/R_{os}} \tag{1}$$

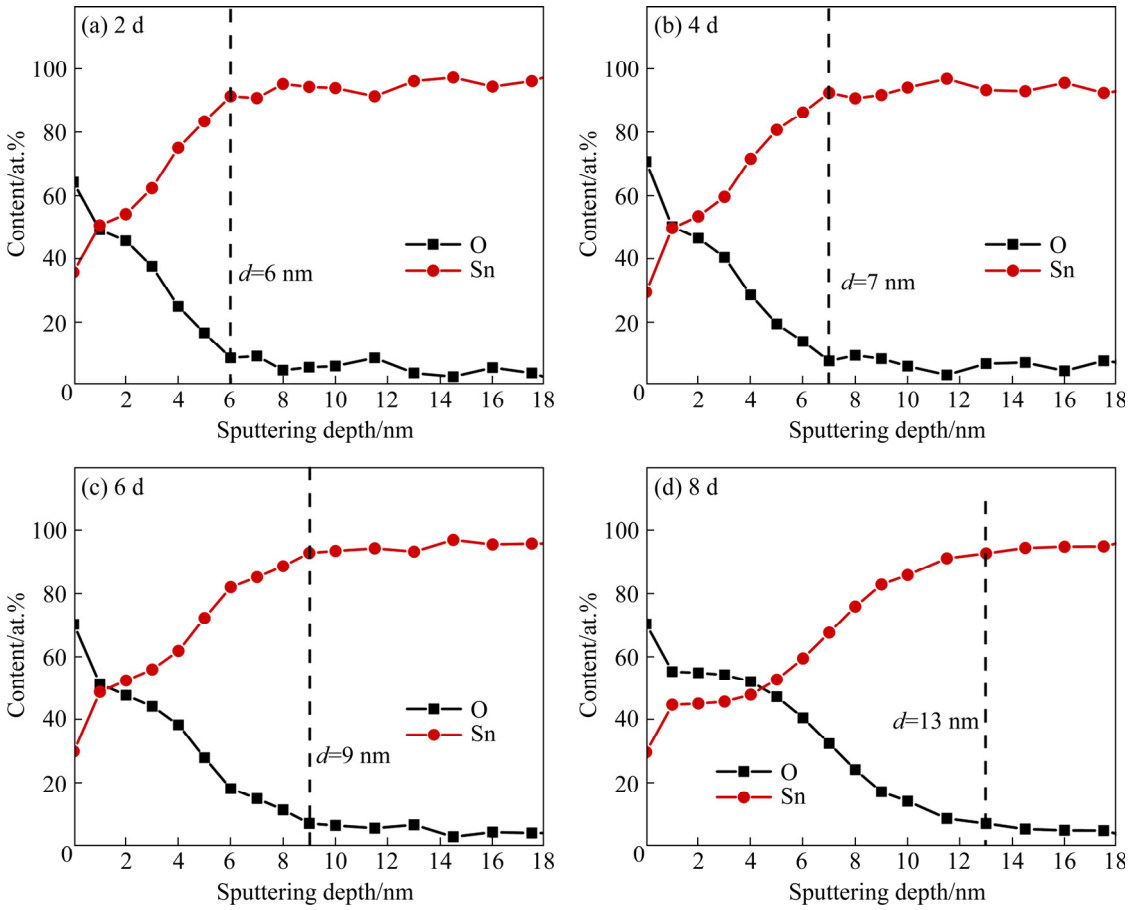

Fig. 7 Content evolution of Sn and O elements as function of sputtering depth in oxide film obtained on pure Sn solder substrate surface with aging time in 150 °C dry atmosphere

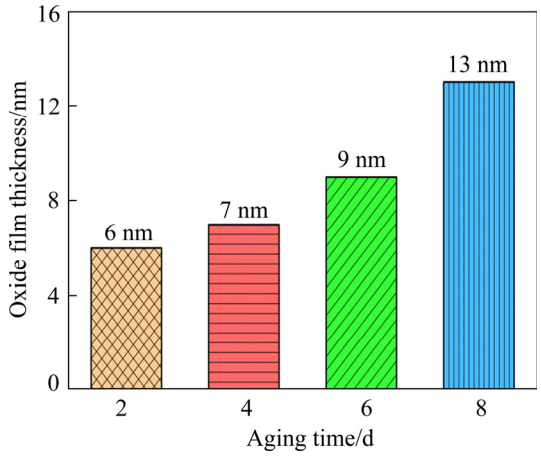

Fig. 8 Derived thickness value of oxide film obtained on pure Sn solder substrate surface with aging time in 150 °C dry atmosphere

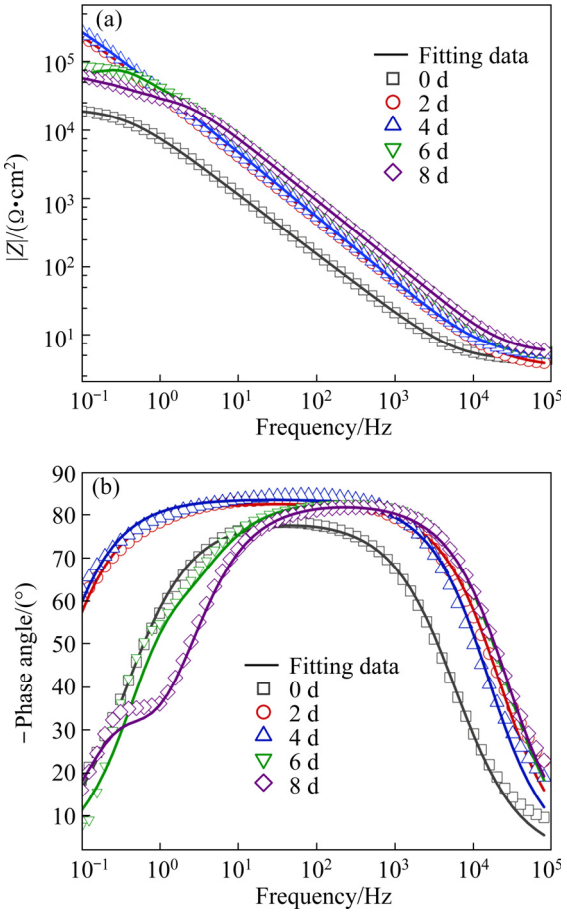

Fig. 9 Bode plots of EIS results for high-temperature aged pure Sn solder substrates exposed to 150 °C dry atmosphere with aging time: (a) Impedance plot; (b) Phase angle plot

$$Z_\omega = R_s + \frac{1}{j\omega Q_{outer} + \frac{1}{R_{outer} + [1/(j\omega Q_{inner} + 1/R_{inner})]}} \quad (2)$$

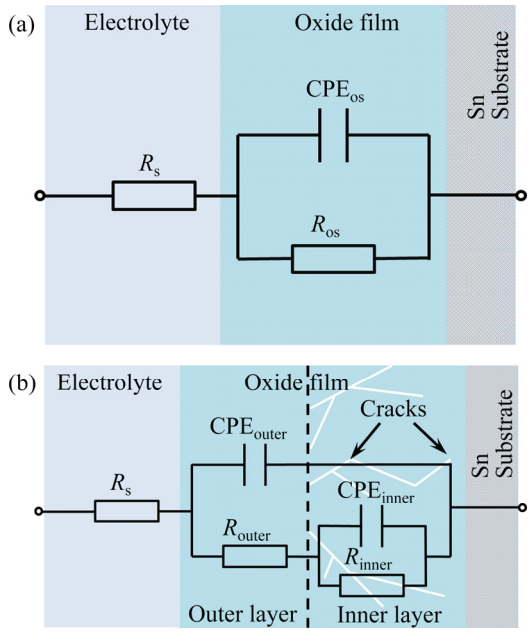

Fig. 10 Equivalent electrical circuit for fitting EIS data of high-temperature aged pure Sn solder substrates with aging time: (a) For samples with aging time of 0, 2 and 4 d; (b) For samples with aging time of 6 and 8 d (R_s is the solution resistance; (CPE (CPE_{os}, CPE_{outer} and CPE_{inner}) and R (R_{os}, R_{outer} and R_{inner}) are the pseudo capacitance and the Faraday resistance caused by the oxide film or the corresponding layer, respectively)

where j is the imaginary unit ($j=(-1)^{0.5}$); ω is the angular frequency; $Z_{CPE}=Q^{-1}(j\omega)^{-n}$ [37], and n (n_{os}, n_{outer} and n_{inner}) indicates the deviation parameter between the equivalent circuit RZ_{CPE} component and the pure RC circuit; and Q can be seen as a true capacitor C when n=1 [37].

The derived parameters of R_s, R_{os}, Q_{os} and n values are shown in Table 2. For the sample without high-temperature aging (0 d), it has a value of R_{os}= 21.09 kΩ·cm^2. Usually, the pre-existing native oxide film on Sn solder substrate surface is less than 5 nm in thickness, and hydroxides, such as $Sn(OH)_4$, $Sn(OH)_2$ and/or $Sn_3O_2(OH)_2$ are often contained [38−40]. When exposed to high-temperature dry atmosphere, these hydroxides undergo dehydration, contributing to the formation of electrochemically stable SnO_2 with an improved corrosion resistance [41]. Therefore, for the sample with an aging time of 2 d, the corrosion resistance is improved greatly with a value of R_{os}=558.3 kΩ·cm^2. As the aging time further proceeds, both the dehydration of hydroxides and the oxidation of fresh Sn solder substrate contribute to the a high

Table 2 Fitting parameters from EIS results of high-temperature aged pure Sn solder substrates (covered with oxide film) measured in 3.5 wt.% NaCl solution using equivalent electrical circuits in Fig. 10

Aging time/d	R_s/($\Omega\cdot cm^2$)	R_{os}/($10^4\Omega\cdot cm^2$)	Q_{os}/($10^{-5}F\cdot cm^{-2}\cdot s^{n-1}$)	n_{os}	$\chi^2/10^{-3}$
0	4.281	2.109	2.250	0.879	0.79
2	3.619	55.83	0.531	0.928	1.99
4	4.940	70.13	0.458	0.931	2.38

Aging time/d	R_s/($\Omega\cdot cm^2$)	R_{outer}/($10^4\Omega\cdot cm^2$)	Q_{outer}/($10^{-5}F\cdot cm^{-2}\cdot s^{n-1}$)	n_{outer}	R_{inner}/($10^4\Omega\cdot cm^2$)	Q_{inner}/($10^{-5}F\cdot cm^{-2}\cdot s^{n-1}$)	n_{inner}	$\chi^2/10^{-4}$
6	5.246	4.960	0.280	0.925	4.025	0.351	0.996	4.86
8	5.391	3.608	0.275	0.923	3.461	2.134	0.987	1.17

χ^2 represents the standard deviation

amount of SnO_2 in the oxide film, and thus a further increased value of R_{os}=701.3 $k\Omega\cdot cm^2$ has been observed for the sample with an aging time of 4 d. However, with the accomplishment of hydroxide dehydration and further oxidation of fresh Sn solder substrate under a thicker oxide film, SnO_2 crystal grows in excessive size, leading to crack formation in the inner layer of the oxide film, and thus a decreased value of R_{os}=89.85 $k\Omega\cdot cm^2$ has been observed for the sample with an aging time of 6 d. As the aging time further proceeds to 8 d, more cracks with an increasing size facilitate the penetration of NaCl electrolyte through the oxide film. Therefore, a further decreased value of R_{os}= 70.69 $k\Omega\cdot cm^2$ has been observed. It can be concluded from such an evolution behavior that high-temperature aging initially improves the corrosion resistance of the oxide film on pure Sn solder substrate and then deteriorates the film structure with a decreasing corrosion resistance to NaCl electrolyte.

As the n value is close to 1, the Q can be directly replaced by a true capacitor C [37], and thus the variation of n value can reflect the compactness of the oxide film. It can also be seen from Table 2 that for the sample without high-temperature aging, it has a value of n=0.879. However, for the samples submitted to high-temperature aging at 150 °C for 2, 4, 6 and 8 d, n values of 0.928, 0.931, 0.925 and 0.923 in sequence have been obtained. The firstly increasing and then decreasing n value of the sample with aging time indicates that high-temperature aging initially improves structure of the pre-existing native oxide film with an increasing corrosion resistance and then deteriorates the structure of the oxide film with a decreasing corrosion resistance. These expectations are in accordance with the surface morphologies observation in Fig. 1 and the EIS results in Fig. 9. In addition, for the samples with aging time of 6 and 8 d in Table 2, n_{inner} has a higher value than n_{outer}, indicating that the inner layer has a better compactness than the outer layer of the oxide film [42]. Usually, the inner compact layer of an oxide film is very thin in thickness, and neglecting the effect of inner oxide film layer thickness, the decreasing value of Q_{outer} in Table 2 indicates an increasing thickness of the oxide film as the high-temperature aging time proceeds. This conclusion is in accordance with the thickness estimation by XPS results in Fig. 8.

3.3.2 Potentiodynamic polarization curve evolution

The above EIS results have shown that high-temperature aging can greatly affect structures of the surface oxide film on pure Sn solder substrate. Potentiodynamic polarization curve has also been used to further characterize the high-temperature aging time induced corrosion resistance evolution of the pure Sn solder substrate, and the obtained curves are displayed in Fig. 11. It can be seen that all the samples show a similar shape in the evolution behavior of obtained polarization curve. In the anodic branch, the anodic current density sharply increases to a maximum value at a potential about −0.4 V (vs SCE), and then shows a fluctuation evolution trend in a narrow range as the potential positively evolves. The same potential value at which all the samples show an abrupt increase in anodic current density not only indicates the bankrupt of the surface oxide film but also implies that all the samples have the same electrochemical characteristics, and the same

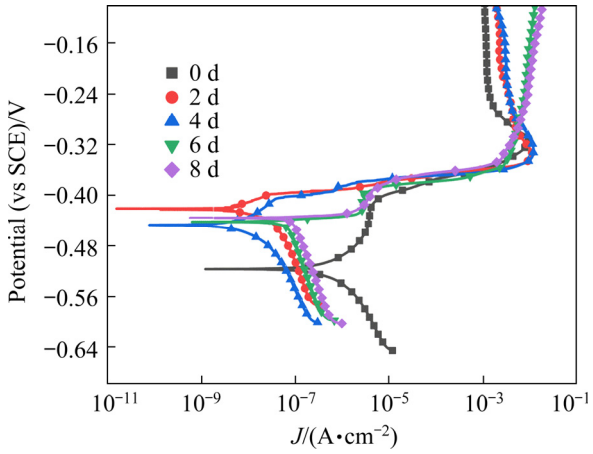

Fig. 11 Potentiodynamic polarization curves of high-temperature aged pure Sn solder substrates with aging time measured in 3.5 wt.% NaCl solution

composition of surface oxide film for all the samples is supposed to be responsible for this [43].

Figure 11 also indicates that in Tafel region of the anodic branch, the anodic current density decreases gradually as the aging time proceeds from 0 to 4 d and then increases as the aging time further extends to 6 and 8 d. For the evolution of cathodic reduction current density, it shows the same evolution behavior as the anodic current density, i.e., it decreases to the lowest value as the aging time proceeds from 0 to 4 d and then gradually increases as the aging time further extends to 6 and 8 d. Therefore, it can be concluded that, for the corrosion of high-temperature aged pure Sn solder substrates in 3.5 wt.% NaCl solution, the high-temperature aging affects not only the anodic dissolution process but also the cathodic reduction process of the samples covered with an oxide film. The cathodic Tafel slope $-\beta_c$ is determined by cathodic Tafel linear fitting and the anodic Tafel slope $-\beta_a$ is determined by anodic Tafel linear fitting [44]. Moreover, the corrosion potential φ_{corr} and the corrosion current density J_{corr} are obtained at the intersection of cathodic Tafel linear fitting and anodic Tafel linear fitting curves [45]. These extracted electrochemical parameters for all the samples with different aging time are listed in Table 3 for discussion.

Table 3 shows that the sample without high-temperature aging has the highest value of J_{corr}=2.07 μA/cm^2, and the 2 d sample has a greatly lowered value of J_{corr}=2.55×10^{-2} μA/cm^2, indicating the increasing resistance to corrosion electrolyte in

Table 3 Electrochemical parameters extracted from the potentiodynamic polarization curves measured on high-temperature aged pure Sn solder substrates (covered with oxide film) in 3.5 wt.% NaCl solution

Aging time/d	φ_{corr}(vs SCE)/mV	β_a/(mV·dec^{-1})	$-\beta_c$/(mV·dec^{-1})	J_{corr}/(μA·cm^{-2})
0	−561	527	129.74	2.07
2	−397	4.98	185.61	0.02550
4	−410	8.50	156.34	0.01242
6	−438	4.26	207.48	0.06661
8	−435	5.68	202.92	0.08761

penetrating through the oxide film to dissolve underlying fresh Sn solder substrate, i.e., the corrosion resistance of the oxides film is enhanced. For the sample with an aging time of 4 d, it has the lowest value of J_{corr}=1.242×10^{-2} μA/cm^2, demonstrating the best compactness of the surface oxide film in resisting penetration of corrosion electrolyte through the oxide film to underlying fresh Sn solder substrate. However, for the sample with an aging time of 6 d, J_{corr} increases to a higher value of 6.661×10^{-2} μA/cm^2, indicating the deterioration in structures of the oxide film with extending high-temperature aging time. The J_{corr} further increases to a value of 8.761×10^{-2} μA/cm^2 for the sample with an aging time of 8 d, and the further deterioration in film structures with more cracks caused by excessive growth of SnO_2 crystals in size is supposed to be responsible for this. Therefore, it can be concluded that high-temperature aging initially enhances the corrosion resistance of surface oxide film and then deteriorates the film structures with a decreasing resistance to 3.5 wt.% NaCl solution.

3.4 Effect of high-temperature aging

For the electrochemical corrosion of pure Sn solder substrate in room temperature atmosphere even with a lower relative humidity (RH), the involved main anodic reaction and cathodic reaction can be expressed by Reaction (3) and Reaction (4), respectively:

$$Sn \rightarrow Sn^{2+}+2e \quad (3)$$

$$2H_2O+O_2+4e \rightarrow 4OH^- \quad (4)$$

The generated Sn^{2+} undergoes hydrolysis, contributing to hydroxide formation as shown by Reaction (5):

$$Sn^{2+}+2OH^- \rightarrow Sn(OH)_2 \quad (5)$$

The produced $Sn(OH)_2$ ($\Delta_f G_m^\Theta$ (298.15 K)=(−462.32±0.66) kJ/mol) can be easily oxidized into $Sn(OH)_4$ ($\Delta_f G_m^\Theta$ (298.15 K)=(−944.93±0.66) kJ/mol) under the effect of H_2O molecules and oxygen as indicated by Reaction (6) [46,47]:

$$2Sn(OH)_2+2H_2O+O_2\rightarrow 2Sn(OH)_4 \quad (6)$$

Both $Sn(OH)_2$ and $Sn(OH)_4$ can be dehydrated into oxides in atmosphere especially with a decreasing value in RH and/or an increasing value in temperature as shown by Reaction (7) and Reaction (8):

$$Sn(OH)_2\rightarrow SnO+H_2O \quad (7)$$

$$Sn(OH)_4\rightarrow SnO_2+2H_2O \quad (8)$$

Meanwhile, the obtained SnO ($\Delta_f G_m^\Theta$ (298.15 K)=(−255.44±0.76) kJ/mol) can be easily oxidized into SnO_2 ($\Delta_f G_m^\Theta$ (298.15 K)=(−511.87±0.78) kJ/mol) with a ready oxygen availability as shown by Reaction (9) [12,48]:

$$2SnO+O_2\rightarrow 2SnO_2 \quad (9)$$

Therefore, at room temperature, the formed native oxide film on pure Sn solder substrate is supposed to have a layered structure with the outer layer composed of more $Sn(OH)_4$ and less SnO_2 and the inner layer composed of more SnO and less $Sn(OH)_2$ [49]. Such an expectation in the pre-existing native oxide film structure is in accordance with the investigation reported by QIAO et al [12]. At this time, the oxide film is very thin in thickness, and the surface morphology is uniform and smooth as seen in Fig. 1(a) and has a lower value of surface roughness S_a=74 nm as shown in Fig. 2(a). However, as the film at this time has a lower content of SnO_2, it has a lower corrosion resistance to NaCl electrolyte penetration as indicated by the lower oxide film resistance value of 21.09 kΩ·cm^2 in Table 2 and the highest corrosion current density value of 2.07 μA/cm^2 in Table 3.

When the pure Sn solder substrate covered with native oxide film is exposed to 150 °C dry atmosphere, the high-temperature induced dehydration in hydroxides deteriorates the surface integrity of the oxide film, and thus a gravel-like rough surface morphology with a larger gravel diameter has been observed for the sample with an aging time of 2 d in Fig. 1(b) and the surface roughness increases greatly to 112 nm in Fig. 2(b). However, the high-temperature aging induced dehydration processes accelerate the transformation of $Sn(OH)_4$ to form SnO_2 and $Sn(OH)_2$ to form SnO. Moreover, the oxidation of fresh Sn substrate (at a lower rate during initial aging duration) and SnO can also contribute to a higher content of SnO_2 in the oxide film as indicated by Reactions (10)−(12):

$$Sn+1/2O_2\rightarrow SnO \quad (10)$$

$$SnO+1/2O_2\rightarrow SnO_2 \quad (11)$$

$$Sn+O_2\rightarrow SnO_2 \quad (12)$$

The decreasing content of $Sn(OH)_4$ and increasing content of SnO_2 in the oxide film contribute to an improved corrosion resistance of the sample with an aging time of 2 d as indicated by the higher oxide film resistance of 558.3 kΩ·cm^2 in Table 2 and the greatly lowered corrosion current density value of 2.55×10^{-2} μA/cm^2 in Table 3. As the high-temperature aging time increases to 4 d, the dehydration process and the growth of SnO_2 crystals further deteriorate the integrity of surface oxide film with a decreasing gravel diameter observed in Fig. 1(c) and the surface roughness further increases to 166 nm in Fig. 2(c). Besides, the oxidation of fresh Sn solder substrate is enhanced and the oxide film thickness begins to increase at a higher rate as seen in Fig. 8. Similarly, the increasing content of SnO_2 in the oxide film further enhances corrosion resistance of the sample as indicated by the higher oxide film resistance of 701.3 kΩ·cm^2 in Table 2 and the further lowered corrosion current density value of 1.242×10^{-2} μA/cm^2 in Table 3. Nevertheless, when the high-temperature aging time increases to 6 d, the excessive growth of SnO_2 crystals in size and the further oxidation of fresh Sn solder substrate lead to a greater thickness of surface oxide film but with the formation of inner cracks [50], and thus a greatly decreased oxide film resistance of 89.85 kΩ·cm^2 in Table 2 and the greatly increased corrosion current density value of 6.661×10^{-2} μA/cm^2 in Table 3 have been observed. For the sample with an aging time of 8 d, the oxide film thickness further increases but with more cracks in the oxide film caused by further growth of SnO_2 crystals in size, and thus a further decreased oxide film resistance of 70.69 kΩ·cm^2 in Table 2 and a further increased corrosion current density value of 8.761×10^{-2} μA/cm^2 in Table 3 have been found.

To sum up, high-temperature aging initially deteriorates surface integrity of the pre-existing

native oxide film, facilitates the dehydration of hydroxides and the oxidation of fresh pure Sn substrate with an increasing content of SnO_2 in the oxide film. Therefore, an increasing thickness in the oxide film with an improved corrosion resistance has been observed during the initial agi1ng duration. Although an extended aging duration always contributes to an increasing thickness of the oxide film, the oversize growth of SnO_2 crystals leads to more cracks inside the oxide film and thus deteriorates the film resistance to NaCl electrolyte. Therefore, the high-temperature aging process has a great influence on the surface integrity, composition and structure, thickness and corrosion resistance of the oxide film on pure Sn solder substrate.

4 Conclusions

(1) High-temperature aging accelerates the dehydration of $Sn(OH)_4$ in the pre-existing native oxide film to form SnO_2 and facilitates the oxidation of fresh Sn substrate, leading to increasing thickness of the surficial oxide film. Meanwhile, the dehydration of pre-existing native oxide film and the gradual growth of SnO_2 crystals make Sn substrate with an increasing surface roughness.

(2) High-temperature aging time initially improves and then deteriorates corrosion resistance of the surface oxide film on pure Sn solder substrate in 3.5 wt.% NaCl solution. The increasing SnO_2 content in the film and the gradual formation of microcracks by oversize growth of SnO_2 crystals are responsible for such a corrosion evolution behavior of the high-temperature aged Sn solder substrate.

Acknowledgments

The financial support from CAS Key Laboratory of Nuclear Materials and Safety Assessment, Institute of Metal Research, Chinese Academy of Sciences, is gratefully acknowledged.

References

[1] ZHANG Xiang-zhao, WU Xiao-liang, LIU Gui-wu, LUO Wen-qiang, GUO Ya-jie, QIAO Guan-jun. Wetting of molten Sn−3.5Ag−0.5Cu on Ni−P(−SiC) coatings deposited on high volume faction SiC/Al composite [J]. Transactions of Nonferrous Metals Society of China, 2018, 28: 1784−1792.

[2] ZHONG Xian-kang, ZHANG Guo-an, QIU Yu-bin, CHEN Zhen-yu, GUO Xing-peng, FU Chao-yang. The corrosion of tin under thin electrolyte layers containing chloride [J]. Corrosion Science, 2013, 66: 14−25.

[3] TUNTHAWIROON P, KANLAYASIRI K. Effects of Ag contents in Sn–*x*Ag lead-free solders on microstructure, corrosion behavior and interfacial reaction with Cu substrate [J]. Transactions of Nonferrous Metals Society of China, 2019, 29(8): 1696−1704.

[4] CHANTARAMANEE S, SUNGKHAPHAITOON P. Influence of bismuth on microstructure, thermal properties, mechanical performance, and interfacial behavior of SAC305−*x*Bi/Cu solder joints [J]. Transactions of Nonferrous Metals Society of China, 2021, 31(5): 1397−1410.

[5] WANG Ming-na, WANG Jian-qiu, KE Wei. Corrosion behavior of Sn−3.0Ag−0.5Cu lead-free solder joints [J]. Microelectronics Reliability, 2017, 73: 69−75.

[6] TIAN Shuang, LIU Yu-shuang, MA Qiang, ZHANG Pei-gen, ZHOU Jian, XUE Feng, SUN Zheng-ming. Intermetallics-induced directional growth of Sn whiskers in Sn−3.5Ag coating on Al substrate [J]. Applied Surface Science, 2021, 539: 148135.

[7] GAO Yan-fang, CHENG Cong-qian, ZHAO Jie, WANG Li-hua, LI Xiao-gang. Electrochemical corrosion of Sn−0.75Cu solder joints in NaCl solution [J]. Transactions of Nonferrous Metals Society of China, 2012, 22(4): 977−982.

[8] YI Pan, DONG Chao-fang, XIAO Kui, LI Xiao-gang. Study on corrosion behavior of β-Sn and intermetallic compounds phases in SAC305 alloy by in-situ EC-AFM and first-principles calculation [J]. Corrosion Science, 2021, 181: 109244.

[9] WANG Ming-na, WANG Jian-qiu, FENG Hao, KE Wei. Effect of Ag_3Sn intermetallic compounds on corrosion of Sn−3.0Ag−0.5Cu solder under high-temperature and high-humidity condition [J]. Corrosion Science, 2012, 63: 20−28.

[10] WANG Ming-Na, WANG Jian-qiu, KE Wei. Corrosion behavior of Sn−3.0Ag−0.5Cu solder under high-temperature and high-humidity condition [J]. Journal of Materials Science: Materials in Electronics, 2014, 25: 1228−1236.

[11] QIAO Chuang, WANG Ming-na, HAO Long, JIANG Xiao-lin, LIU Xia-he, THEE C, AN Xi-zhong. In-situ EIS study on the initial corrosion evolution behavior of SAC305 solder alloy covered with NaCl solution [J]. Journal of Alloys and Compounds, 2021, 852: 156953.

[12] QIAO Chuang, SUN Xu, WANG You-zhi, HAO Long, LIU Xia-he, AN Xi-zhong. High-temperature aging time-induced composition and thickness evolution in the native oxides film on Sn solder substrate [J]. Journal of Materials Science: Materials in Electronics, 2021, 32: 24209−24228.

[13] LIU Yang, JIAO Yang, ZHANG Zheng-lin, QU Feng-yu, UMAR A, WU Xiang. Hierarchical SnO_2 nanostructures made of intermingled ultrathin nanosheets for environmental remediation, smart gas sensor, and supercapacitor applications [J]. ACS Applied Materials & Interfaces, 2014, 6(3): 2174−2184.

[14] WANG H K, ROGACH A L. Hierarchical SnO_2 nanostructures: Recent advances in design, synthesis, and applications [J]. Chemistry of Materials, 2014, 26: 123−133.

[15] QIAO Chuang, SUN Xu, WANG You-zhi, HAO Long, AN

Xi-zhong. A perspective on effect by Ag addition to corrosion evolution of Pb-free Sn solder [J]. Materials Letters, 2021, 297: 129935.

[16] WU Ming, WANG Shan-lin, SUN Wen-jun, HONG Min, CHEN Yu-hua, KE Li-ming. Fracture pattern evolution of SnAgCu−SnPb mixed solder joints at cryogenic temperature [J]. Transactions of Nonferrous Metals Society of China, 2021, 31: 2760−2772.

[17] WANG Ming-na, QIAO Chuang, JIANG Xiao-lin, HAO Long, LIU Xai-he. Microstructure induced galvanic corrosion evolution of SAC305 solder alloys in simulated marine atmosphere [J]. Journal of Materials Science & Technology, 2020, 51: 40−53.

[18] CHEN G, WANG X H, YANG J, XU W L, LIN Q. Effect of micromorphology on corrosion and mechanical properties of SAC305 lead-free solders [J]. Microelectronics Reliability, 2020, 108: 113634.

[19] TU Xiao-xuan, YI Dan-qing, WU Jing, WANG Bin. Influence of Ce addition on Sn−3.0Ag−0.5Cu solder joints: Thermal behavior, microstructure and mechanical properties [J]. Journal of Alloys and Compounds, 2017, 698: 317−328.

[20] SATIZABAL L M, COSTA D, MORAES P B, BORTOLOZO A D, OSÓRIO W R. Microstructural array and solute content affecting electrochemical behavior of SnAg and SnBi alloys compared with a traditional SnPb alloy [J]. Materials Chemistry and Physics, 2019, 223: 410−425.

[21] HAN Yong-dian, YANG Jia-hang, XU Lian-yong, JING Hong-yang, ZHAO Lei. Effect of transient current bonding on interfacial reaction in Ag-coated graphene Sn−Ag−Cu composite solder joints [J]. Transactions of Nonferrous Metals Society of China, 2021, 31: 2454−2467

[22] SZUBER J, CZEMPIK G, LARCIPRETE R, KOZIEJ D, ADAMOWICZ B. XPS study of the L-CVD deposited SnO_2 thin films exposed to oxygen and hydrogen [J]. Thin Solid Films, 2001, 391: 198−203.

[23] LI De-zhi, CONWAY P P, LIU Chang-qing. Corrosion characterization of tin-lead and lead free solders in 3.5 wt.% NaCl solution [J]. Corrosion Science, 2008, 50: 995−1004.

[24] LIU Jian-chun, ZHANG Gong, NAGAO S, JIU Jin-ting, NOGI M, SUGAHARA T, MA Ju-sheng, SUGANUMA K. Metastable pitting and its correlation with electronic properties of passive films on Sn–*x*Zn solder alloys [J]. Corrosion Science, 2015, 99: 154−163.

[25] XIA Da-hai, QIN Zhen-bo, SONG Shi-zhe, MACDONALD D, LUO Jing-li. Combating marine corrosion on engineered oxide surface by repelling, blocking and capturing Cl^-: A mini review [J]. Corrosion Communications, 2021, 2: 1−8.

[26] ZHANG Sha-sha, ZHANG Yi-jie, WANG Hao-wei. Effect of oxide thickness of solder powders on the coalescence of SnAgCu lead-free solder pastes [J]. Journal of Alloys and Compounds, 2009, 487: 682−686.

[27] GARDIN E, ZANNA S, SEYEUX A, ALLION-MAURER A, MARCUS P. XPS and ToF-SIMS characterization of the surface oxides on lean duplex stainless steel—Global and local approaches [J]. Corrosion Science, 2019, 155: 121−133.

[28] KWOKA M, OTTAVIANO L, PASSACANTANDO M, SANTUCCI S, SZUBER J. XPS depth profiling studies of L-CVD SnO_2 thin films [J]. Applied Surface Science, 2006, 252: 7730−7733.

[29] CHAN-ROSADO G, PECH-CANUL M A. Influence of native oxide film age on the passivation of carbon steel in neutral aqueous solutions with a dicarboxylic acid [J]. Corrosion Science, 2019, 153: 19−31.

[30] CHASTAIN J, KING R C Jr. Handbook of X-ray photoelectron spectroscopy [M]. Eden Prairie, Minnesota: Perkin-Elmer Corporation, 1992: 261.

[31] XIA Da-hai, SONG Shi-zhe, TAO Lei, QIN Zhen-bo, WU Zhong, GAO Zhi-ming, WANG Ji-hui, HU Wen-bin, BEHNAMIAN Y, LUO Jing-li. Review-material degradation assessed by digital image processing: Fundamentals, progresses, and challenges [J]. Journal of Materials Science & Technology, 2020, 53(18): 146−162.

[32] JUNG J Y, LEE S B, JOO Y C, LEE H Y, PARK Y B. Anodic dissolution characteristics and electrochemical migration lifetimes of Sn solder in NaCl and Na_2SO_4 solutions [J]. Microelectronic Engineering, 2008, 85: 1597−1602.

[33] XIE Shi-jing, SONG Wen-xiong, ZHOU Bang-xin, XU Jing, ZHAO Shi-jin. Study of the anisotropic segregation behavior of Sn on the surfaces of zirconium alloys by XPS [J]. Applied Surface Science, 2015, 356: 769−775.

[34] PAN Cheng-cheng, SONG Yang, JIN Wei-xian, SONG Shi-zhe HU Wen-bing, XIA Da-hai. Enhancing the stability of passive film on 304 SS by chemical modification in alkaline phosphate–molybdate solutions [J]. Transactions of Tianjin University, 2020, 26(2): 135−141.

[35] LIU Jian-chun, ZHANG Gong, MA Ju-sheng, SUGANUMA K. Ti addition to enhance corrosion resistance of Sn−Zn solder alloy by tailoring microstructure [J]. Journal of Alloys and Compounds, 2015, 644: 113−118.

[36] MANSFELD F, TSAI C H. Determination of coating deterioration with EIS: I. Basic relationships [J]. Corrosion, 1991, 47: 958−963.

[37] ORAZEM M E, TRIBOLLET B. Electrochemical impedance spectroscopy [M]. New Jersey: John Wiley & Sons, 2008: 383−389.

[38] ECKOLD P, ROLFF M, NIEWA R, HÜGEL W. Synthesis, characterization and in situ Raman detection of $Sn_3O_2(OH)_{2-x}Cl_x$ phases as intermediates in tin corrosion [J]. Corrosion Science, 2015, 98: 399−405.

[39] MOHANTY U S, LIN K L. The effect of alloying element gallium on the polarization characteristics of Pb-free Sn−Zn−Ag−Al−*X*Ga solders in NaCl solution [J]. Corrosion Science, 2006, 48: 662−678.

[40] KAPUSTA S D, HACKERMAN N. Anodic passivation of tin in slightly alkaline solutions [J]. Electrochimica Acta, 1980, 25: 1625−1639.

[41] MOHANTY U S, LIN K L. Effect of Al on the electrochemical corrosion behavior of Pb free Sn−8.5Zn−0.5Ag−*X*Al−0.5Ga solder in 3.5% NaCl solution [J]. Applied Surface Science, 2006, 252: 5907−5916.

[42] LIAO Bo-kai, CEN Hong-yu, CHEN Zhen-yu, GUO Xing-peng. Corrosion behavior of Sn−3.0Ag−0.5Cu alloy under chlorine-containing thin electrolyte layers [J]. Corrosion Science, 2018, 143: 347−361.

[43] BATZILL M, DIEBOLD U. The surface and materials science of tin oxide [J]. Progress in Surface Science, 2005,

79: 47−154.

[44] JYOTHEENDER K S, KUMAR M K P, SRIVASTAVA C. Low temperature electrogalvanization: Texture and corrosion behavior [J]. Applied Surface Science, 2021, 559: 149953.

[45] MOHANTY U S, LIN K L, Electrochemical corrosion behaviour of Pb-free Sn−8.5Zn−0.05Al−*X*Ga and Sn−3Ag−0.5Cu alloys in chloride containing aqueous solution [J]. Corrosion Science, 2008, 50: 2437−2443.

[46] TSAO L. Corrosion resistance of Pb-free and novel nano-composite solders in electronic packaging [M]. Rijeka, Croatia: InTech, 2012.

[47] LAO Xiao-dong, CHENG Cong-qian, MIN Xiao-hua, ZHAO Jie, ZHOU Da-yu, WANG Li-hua, LI Xiao-gang. Corrosion and leaching behaviors of Sn-based alloy in simulated soil solutions [J]. Transactions of Nonferrous Metals Society of China, 2016, 26(2): 581−588.

[48] XIA Da-hai, SONG Shi-zhe, QIN Zhen-bo, HU Wen-bin, BEHNAMIAN Y. Review—Electrochemical probes and sensors designed for time-dependent atmospheric corrosion monitoring: Fundamentals, progress, and challenges [J]. Journal of the Electrochemical Society, 2020, 167(3): 037513.

[49] QIAO Chuang, WANG Ming-na, HAO Long, LIU Xia-he, JIANG Xiao-lin, AN Xi-zhong, LI Duan-yang. Temperature and NaCl deposition dependent corrosion of SAC305 solder alloy in simulated marine atmosphere [J]. Journal of Materials Science & Technology, 2021, 75: 252−264.

[50] XIA D H, SONG S Z, BEHNAMIAN Y, HU W B, CHENG Y F, LUO J L, HUET F. Review—Electrochemical noise applied in corrosion science: Theoretical and mathematical models towards quantitative analysis [J]. Journal of the Electrochemical Society, 2020, 167(8): 081507.

纯 Sn 焊料表面高温氧化膜的腐蚀演化行为

赵 晖[1]，孙 旭[1,2]，郝 龙[2,3]，王俭秋[2,3]，杨景梅[4]

1. 沈阳理工大学 材料科学与工程学院，沈阳 110159；
2. 中国科学院 金属研究所 中国科学院核用材料与安全评价重点实验室，沈阳 110016；
3. 中国科学技术大学 材料科学与工程学院，合肥 230026；
4. 沈阳飞机工业(集团)有限公司，沈阳 110034

摘 要：对 150 ℃高温时效条件下纯锡焊料表面氧化膜形貌、组成、厚度及耐蚀性的演化行为进行研究。结果表明，高温时效加速焊料表面原有自然氧化膜层中的 $Sn(OH)_4$ 向 SnO_2 转变，同时加速新鲜 Sn 基体的氧化，从而使纯 Sn 焊料表面氧化膜厚度和粗糙度随时效时间的延长逐渐增加。然而，表面氧化膜层的耐蚀性随时效时间的延长呈先增强而后减弱的趋势。此外，还对纯 Sn 焊料表面氧化膜层的成膜机制及膜层演化机制进行讨论。

关键词：纯锡焊料；氧化膜层；高温时效；耐腐蚀性

(Edited by Wei-ping CHEN)